Journal of Oceanography, Vol. 62, pp. 47 to 61, 2006

Observation of the Soya Warm Current Using HF Ocean Radar

NAOTO EBUCHI*, YASUSHI FUKAMACHI, KAY I. OHSHIMA, KUNIO SHIRASAWA, MASAO ISHIKAWA, TORU TAKATSUKA, TAKAHARU DAIBO† and MASAAKI WAKATSUCHI

Institute of Low Temperature Science, Hokkaido University, Kita-ku, Sapporo 060-0819, Japan

(Received 12 January 2005; in revised form 28 June 2005; accepted 1 August 2005)

Three High Frequency (HF) ocean radar stations were installed around the Soya/La Perouse Strait in the Sea of Okhotsk in order to monitor the Soya Warm Current (SWC). The frequency of the HF radar is 13.9 MHz, and the range and azimuth resolutions are 3 km and 5 deg., respectively. The radar covers a range of approximately 70 km from the coast. The surface current velocity observed by the HF radars was compared with data from drifting buoys and shipboard Acoustic Doppler Current Profilers (ADCPs). The current velocity derived from the HF radars shows good agreement with that observed using the drifting buoys. The root-mean-square (rms) differences were found to be less than 20 cm s^{-1} for the zonal and meridional components in the buoy comparison. The observed current velocity was also found to exhibit reasonable agreement with the shipboard ADCP data. It was shown that the HF radars clearly capture seasonal and short-term variations of the SWC. The velocity of the Soya Warm Current reaches its maximum, approximately 1 m s^{-1}, in summer and weakens in winter. The velocity core is located 20 to 30 km from the coast, and its width is approximately 40 km. The surface transport by the SWC shows a significant correlation with the sea level difference along the strait, as derived from coastal tide gauge records at Wakkanai and Abashiri.

Keywords:
- HF radar,
- Soya Warm Current,
- Sea of Okhotsk,
- coastal current.

1. Introduction

The Sea of Okhotsk (Fig. 1), a marginal sea adjacent to the North Pacific, is one of the southernmost seasonal sea ice zones in the Northern Hemisphere and it has been conjectured that it is a region in which North Pacific Intermediate Water is ventilated to the atmosphere (Talley, 1991; Yasuda, 1997). The Sea of Okhotsk is connected with the Sea of Japan through the Soya/La Perouse Strait, which is located between Hokkaido, Japan, and Sakhalin, Russia. The Soya Warm Current (referred to as SWC hereafter) enters the Sea of Okhotsk from the Sea of Japan through the Soya/La Perouse Strait and flows along the coast of Hokkaido as a coastal boundary current. It supplies warm, saline water in the Sea of Japan to the Sea of Okhotsk. The current is roughly barotropic and shows a clear seasonal variation (Aota, 1984; Matsuyama *et al.*, 1999). The SWC has never been continuously monitored due to the difficulties involved in field observations related to, for example, severe weather conditions in the winter, political issues at the border strait, and conflicts with fishing activities in the strait. Detailed features of the SWC and its variations have not yet been clarified. Information concerning the variations of the SWC and the water exchange between the Sea of Japan and the Sea of Okhotsk is important for the study of both of these seas.

In order to continuously monitor the SWC in and around the Soya Strait, three High Frequency (HF) radars were installed around the Soya Strait (Fig. 1) in March 2003, and continuous observation was started in August 2003. The HF radar has been demonstrated to be a useful tool for the observation of spatial and temporal variations of surface current vectors in coastal regions (e.g., Barrick *et al.*, 1977; Prandle, 1991; Takeoka *et al.*, 1995). The present study analyzes data obtained at these stations over a period of 12 months, from August 2003 to July 2004. The HF radars and stations are described briefly in Section 2. In Sections 3 and 4, the surface current velocity measured by the HF radars is compared to observations obtained by drifting buoys and shipboard Acoustic Doppler Current Profilers (ADCPs), respectively. The

* Corresponding author. E-mail: ebuchi@lowtem.hokudai.ac.jp

† Deceased.

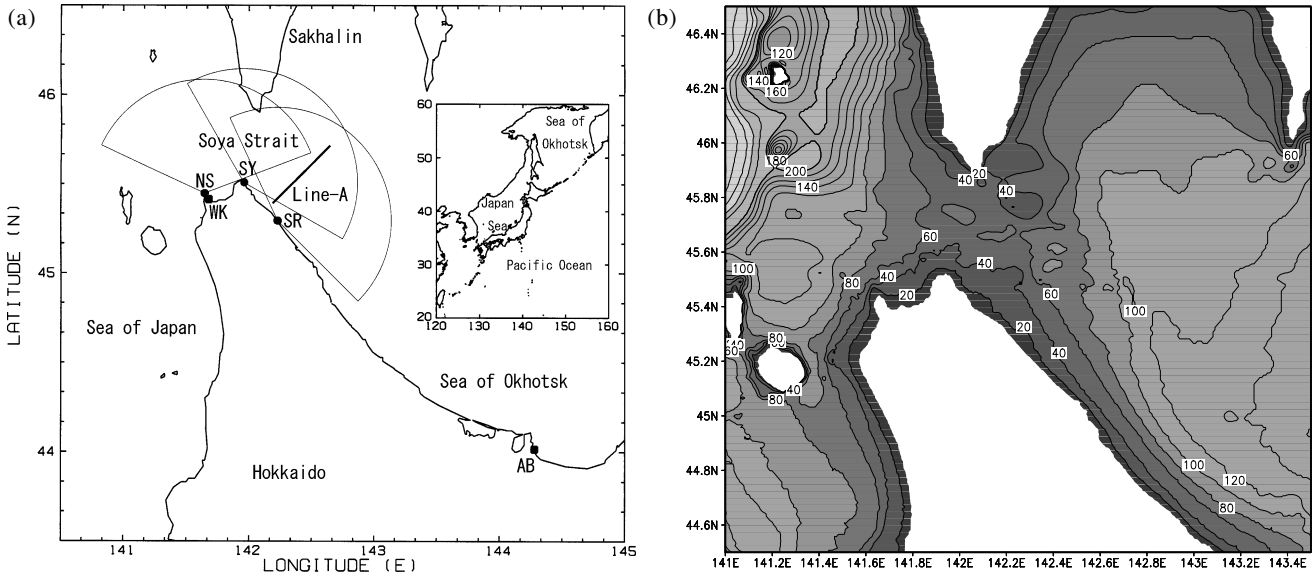

Fig. 1. (a) Map of the Soya/La Perouse Strait, location and coverage of the HF radar stations (NS: Noshappu radar station, SY: Soya radar station, SR: Sarufutsu radar station), and location of the tide gauge stations (WK: Wakkanai, AB: Abashiri), and (b) bathymetry of the Soya/La Perouse Strait (unit: m).

tidal current in the Soya Strait is described in Section 5. Variations of the Soya Warm Current and their relationship to the sea level difference between the Seas of Japan and Okhotsk are discussed in Section 6. Finally, the paper is summarized in Section 7.

2. Radar and Stations

The three HF radar stations used in this study are located around the Soya Strait at Noshappu, Soya, and Sarufutsu (referred to respectively as NS, SY and SR hereafter) (Fig. 1). A SeaSonde HF-radar system (Barrick *et al.*, 1977; Lipa and Barrick, 1983; Barrick and Lipa, 1997) manufactured by CODAR Ocean Sensors, Ltd. was used. The frequency of the HF radar is 13.9 MHz, and the range and azimuth resolutions are 3 km and 5 deg., respectively. The HF radar covers a range of approximately 70 km from the coast. The estimated coverage of the three radars is shown in Fig. 1. The observations were made at one hourly intervals. The characteristics of the HF radar system are summarized in Table 1. We measured the beam pattern of the receiving antenna and corrected for distortion of the antenna pattern to derive accurate radial velocities. These stations have been operated by the Institute of Low Temperature Science of Hokkaido University since August 2003. Surface current vectors were composed in grid cells of 3 × 3 km using the radial velocity components observed by the radars according to a least squares method. This study analyzes data obtained over a period of 12 months, from August 2003 to July 2004.

Examples of the observed surface current vector field are shown in Fig. 2. Figure 2(a) shows the surface current field derived from the data collected at all three stations, whereas the current field shown in Fig. 2(b) was calculated using data from two stations (SY and SR) due to a lack of data at the NS station at that time. Both figures clearly capture the SWC, which flows from west to east across the Soya Strait and turns toward the southeast along the coast. Figure 2(a) also shows the southward current along the west coast of Sakhalin, as predicted by numerical experiments (Ohshima and Wakatsuchi, 1990; Ohshima, 1994). Figure 2(b) shows a cyclonic eddy observed at the offshore side of the SWC. The generation mechanism of the eddy was also revealed by Ohshima and Wakatsuchi (1990) in terms of the barotropic instability of a two-dimensional jet.

Table 1. Specifications of the Soya Strait Ocean Radar System.

Radar type	FMICW
Center frequency	13.946 MHz
Sweep bandwidth	50 kHz
Frequency sweep interval	0.5 s
Transmission power	80 W (max.), 40 W (ave.)
Range resolution	3.0 km
Azimuth resolution	5 deg.
Current velocity resolution	2.25 cm s^{-1}
Antenna type	Twin monopole (transmitter)
	Single cross loop (receiver)

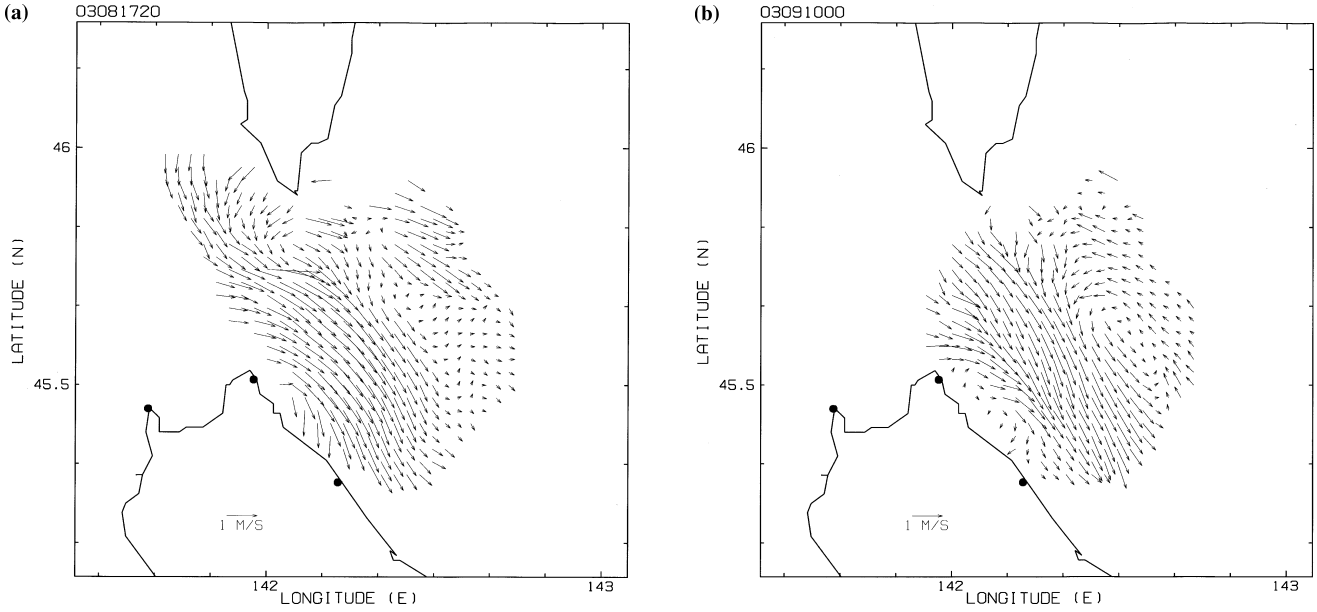

Fig. 2. Two examples of the hourly surface current vector field. (a) 2000 JST, 17 August 2003, and (b) 0000 JST, 10 September 2003. Locations of radar stations are indicated by the solid circles.

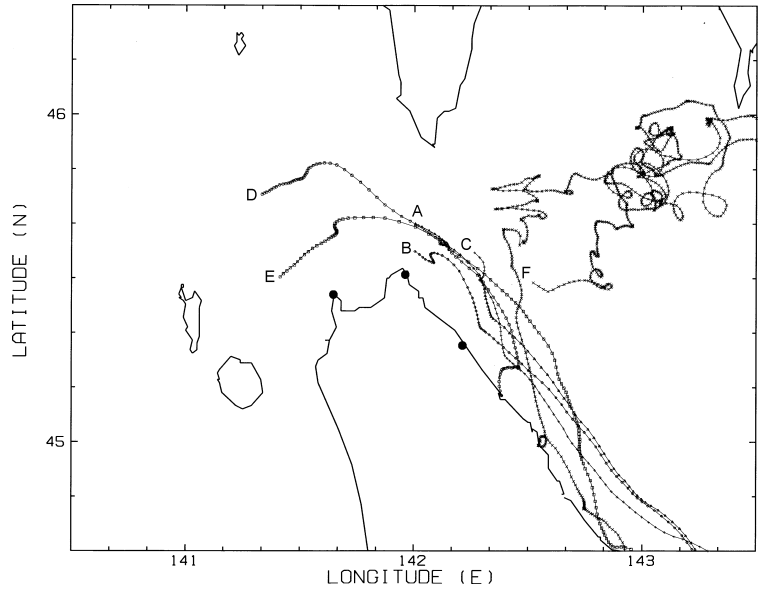

Fig. 3. Hourly locations of drifting buoys. Buoys A, B, and C were deployed on 1 December 2003, Buoys D and E were deployed on 13 April 2004, and Buoy F was deployed on 25 May 2004.

3. Comparison with Data Collected by Drifting Buoys

In order to evaluate the surface current vectors observed by the HF radar system, we deployed a total of six drifting buoys without drogues around the strait in December 2003, April 2004, and May 2004. The drifting buoys (ZTB-R1S4), manufactured by Zeni Lite Buoy Co., Ltd., are 34 cm in diameter, 30 cm in height, and 6.5 kg in weight. The position of each buoy is measured by the Global Positioning System (GPS) and is reported by the Orbcomm satellite system. The temporal interval of the positioning was set to one hour. Figure 3 shows the tra-

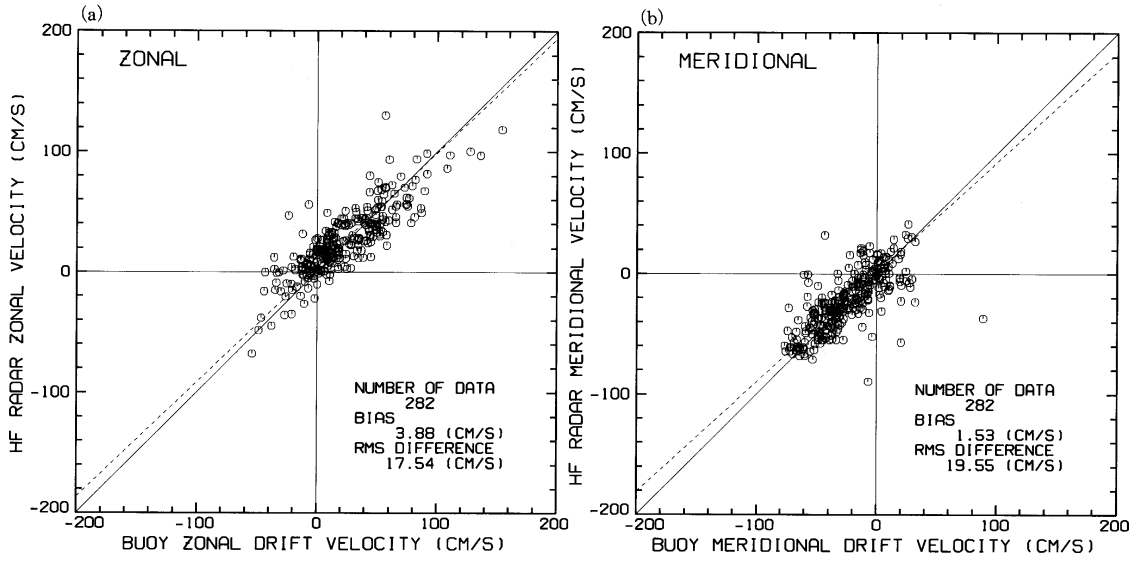

Fig. 4. Comparison of HF radar data with drifting buoy observation data for (a) zonal and (b) meridional components. Dashed lines represent the regression lines calculated using the principal component analysis (PCA).

Table 2. Statistical values of the comparison with drifting buoy observations. Bias is defined as (HF radar – buoy).

	Number of data points	Bias (cm s^{-1})	Rms difference (cm s^{-1})	Correlation coefficient	Slope
Zonal component	282	3.88	17.54	0.844	0.951
Meridional component	282	1.53	19.55	0.710	0.911
Radial component					
NS Station	100	10.20	24.58	0.335	0.811
SY Station	314	4.70	16.22	0.853	0.976
SR Station	583	–1.16	15.57	0.871	0.839

jectories of the buoys. The trajectories of five of the six buoys were near the axis of the SWC. Hourly surface velocity was estimated from the hourly position of the buoys and was collocated with the HF radar observations. Assuming a current speed of a few tenths of a meter per second, the distance traveled by drifting buoys in an hour is estimated to be a few kilometers, which is of the same order as the spatial resolution of the HF radars. The spatial separation between the mean buoy location and the center of the HF radar observation cell is limited to less than 3 km. We obtained 282 collocated data points.

Figure 4 shows the result of comparison between the surface current vectors observed by the HF radars and those inferred from the trajectories of the drifting buoys for the zonal and meridional components. Dashed lines in the panels represent the regression line calculated from principal component analysis (PCA). We utilized PCA rather than simple linear regression, because errors in the current measurements reported by the drifting buoys are not considered to be negligibly small. The number of data points, bias (HF radar – buoy), rms difference, correlation coefficient, and slope of the regression line calculated by the PCA are summarized in Table 2.

Both current components observed by the HF radar show good agreement with the drifting buoy measurements. The biases are negligibly small and rms differences are comparable to or slightly larger than those reported by previous studies in which HF radar observations were compared with in-situ data (e.g., Stewart and Joy, 1974; Barrick *et al.*, 1977; Holbrook and Frisch, 1981; Lawrence and Smith, 1986; Graber *et al.*, 1997; Chapman and Graber, 1997; Chapman *et al.*, 1997; Nadai *et al.*, 1997, 1999). The slopes of the regression line are very close to unity. Considering the fact that the rms difference also arises from errors in the buoy measurements and differences of spatial and temporal averaging of the

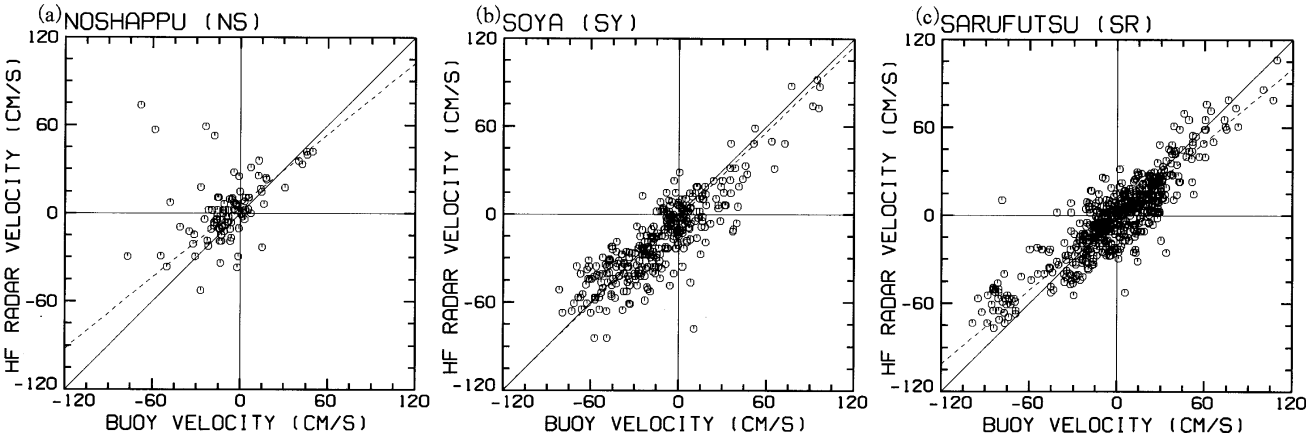

Fig. 5. Comparison of HF radar data with drifting buoy observation data for radial current velocity. (a) NS, (b) SY, and (c) SR stations. Dashed lines represent the regression lines calculated using the PCA.

current velocities, this is small enough to capture the seasonal variations of the SWC, which exceeds a magnitude of 1 m s^{-1} (see Section 6).

The radial velocity components obtained from the three radar stations are compared with the buoy observation data in Fig. 5. The conditions of collocation are the same as for the comparison of the current vectors described above. Statistical values of the comparisons are listed in Table 2. For the SY and SR stations, the radial velocity component agrees well with the buoy observations, with rms differences of 15–16 cm s^{-1}. The correlation coefficients are greater than 0.8, and the slopes of the regression lines are close to unity. For the NS station, however, the scatter of the data points is larger, with an rms difference of 24.58 cm s^{-1}, and the correlation coefficient is very low (0.335), even though the number of data points is less than those obtained at the other stations. The data shown in Fig. 5(a) suggest that the radial velocity observation at the NS station is less accurate than at the other stations. The accuracy of the radial velocity observed at the NS station will be discussed further in the following section. Considering the current directions of the SWC around the NS station (see Figs. 2 and 12), the magnitude of the radial current velocity is relatively small there. This may also reduce the correlation between the NS station and the buoy observations.

4. Comparison with Data Collected by Shipboard ADCPs

The radar-derived surface currents are also compared with shipboard ADCP measurements, which were obtained by patrol ships of the Japan Coast Guard. Typical observation depths range from 5 to 10 m below the surface. The current velocity is reported every five minutes. A three-point running average (over 15 minutes) was applied to the current data in order to match the spatial averaging scale. Assuming a ship velocity of 10 knots (approximately 5 m s^{-1}), the 15-minute average is considered to be equivalent to an average over 4.5 km, which is close to the spatial resolution of the radar observation. We discarded the ADCP data that were obtained during periods when the ship was changing either velocity or heading. The ADCP current data were collocated with the HF radar observations. The spatial separation between the mean ship location and the center of the HF radar observation cell was limited to less than 3 km. We obtained 389 collocated data points. Figure 6 shows the locations of the collocated data points. Most of the data were obtained within distances of 30 km from the coast of Hokkaido.

The results of comparison of the HF radar data with the shipboard ADCP observation data for the zonal and meridional components are shown in Fig. 7. Statistical values of the comparisons are listed in Table 3. Both components show good agreement, although the data exhibit a greater degree of scatter than Fig. 4. The rms differences are increased to 22.93 and 25.66 cm s^{-1} for the zonal and meridional components, respectively. This increase in the rms difference might be explained by the difference of observation depths between the ADCPs (5 to 10 m) and the HF radars (a few meters). In addition, the difference in averaging time (15 min. for ADCP and 1 hour for HF radar) may increase the difference, and the data quality of the ADCP measurements is considered to be poorer than that of the drifting buoys.

In order to assess the effect of the difference in observation depths on the comparison shown in Fig. 7, we investigated the correlation between the current velocity residuals and the wind velocity for the zonal and meridional components. The surface current velocity observed

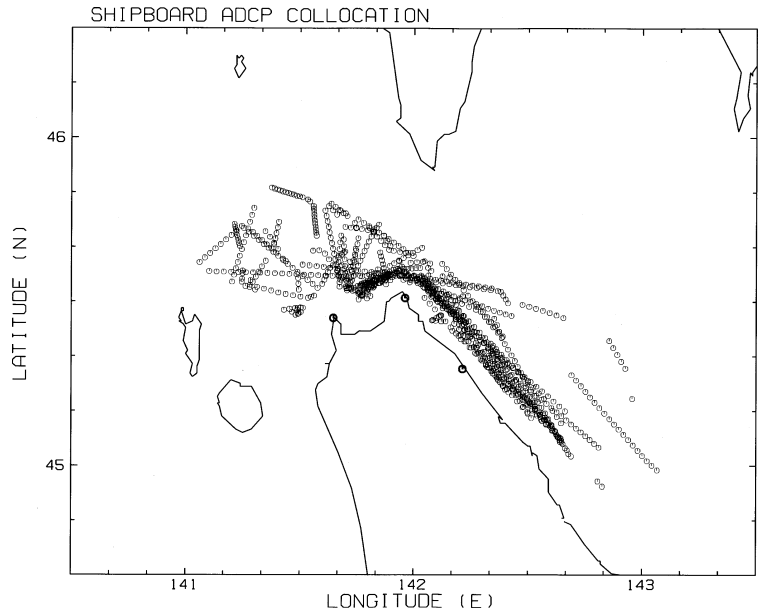

Fig. 6. Locations of shipboard ADCP data points collocated with the HF radar observations.

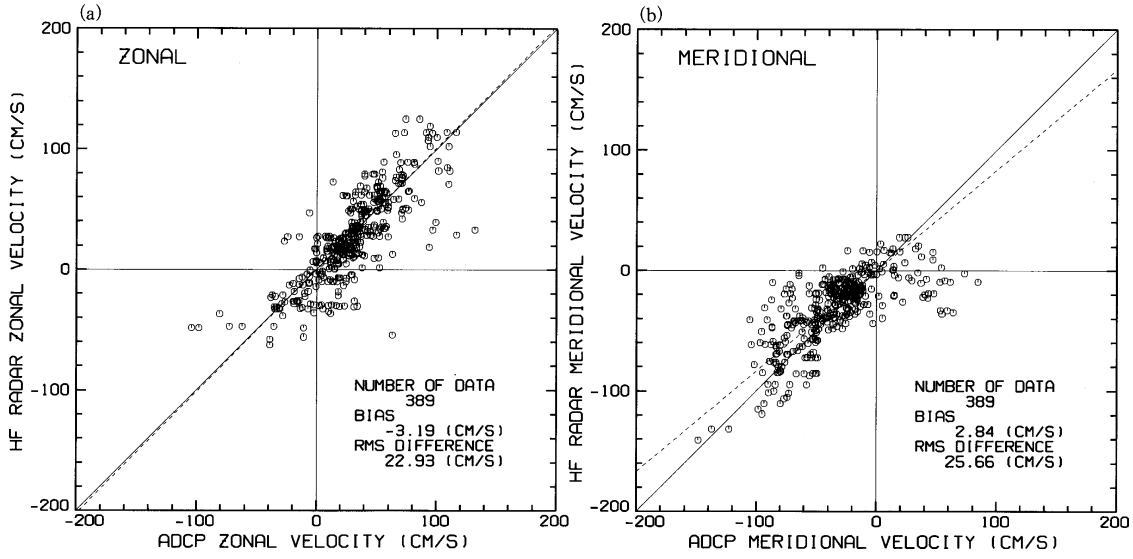

Fig. 7. Comparison of HF radar data with shipboard ADCP observation data for (a) zonal and (b) meridional components. Dashed lines represent the regression lines calculated using the PCA.

by HF radar is considered to be the sum of the mean surface current, tidal current, and wind drift, among which the wind drift component has the largest vertical gradient within a few meters beneath the sea surface. At the current measurement depth of the shipboard ADCPs, which is deeper than that of the HF radars, the wind drift is considered to be much weaker. Figure 8 shows a plot of residuals (HF radar – ADCP) of the zonal and meridional components against the zonal and meridional wind velocity. The wind speed and direction, observed hourly at the Soya-misaki AMeDAS (Automated Meteorological Data Acquisition System) station, located near the SY station (Fig. 1), were temporally interpolated and collocated with the HF radar-ADCP collocated data. A weak positive correlation between the current velocity residual and wind velocity is discernible in both panels of Fig. 8. The

Table 3. Statistical values of the comparison with ADCP observations. Bias is defined as (HF radar – ADCP).

	Number of data points	Bias (cm s^{-1})	Rms difference (cm s^{-1})	Correlation coefficient	Slope
Zonal component	389	–3.19	22.93	0.793	1.011
Meridional component	389	2.84	25.66	0.706	0.833
Radial component					
NS Station	429	–0.74	36.63	0.376	0.289
SY Station	317	2.91	26.62	0.773	1.007
SR Station	481	3.24	25.21	0.853	0.964

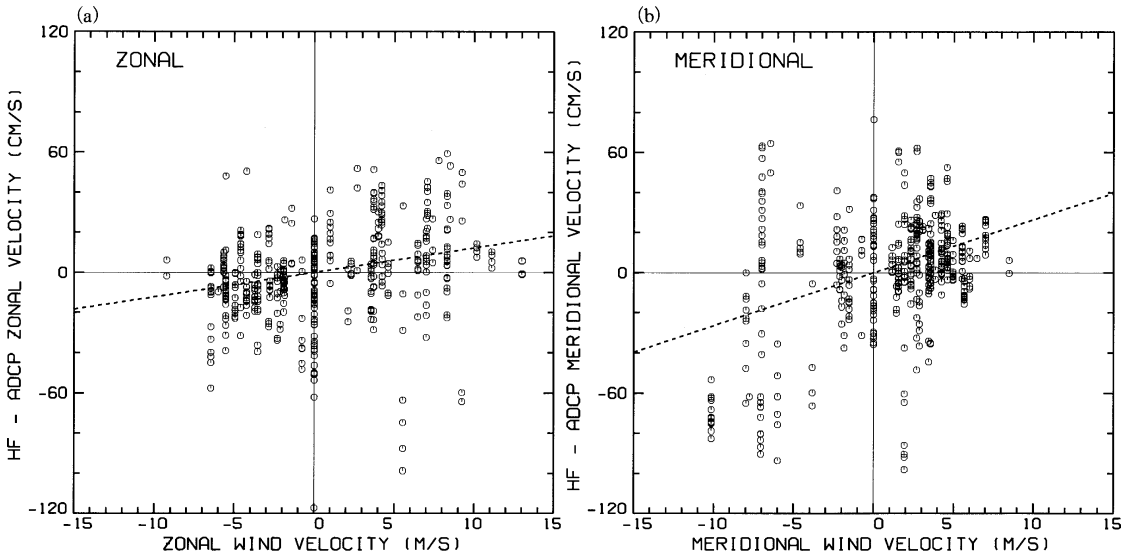

Fig. 8. Comparison of HF radar data for surface current velocity residuals (HF radar – ADCP) of the (a) zonal and (b) meridional components with the zonal and meridional wind velocity observed at the Soya-misaki AMeDAS station, located close to the SY station. Dashed lines represent the linear regression lines.

correlation coefficients are 0.263 and 0.402 for the zonal and meridional components, respectively. These values of correlation coefficients are not very high, even though they are statistically significant, with a 99% confidence limit. Errors in the HF radar and ADCP observations may reduce the correlation. In addition, the wind speed and direction observed at the coastal station may not accurately represent the offshore conditions. The slopes of linear regression lines fitted to the data in Fig. 8 are 0.0122 and 0.0264 for the zonal and meridional components, respectively. These values are consistent with the typical magnitude of the wind drift, which is generally considered to be a few percent of the wind speed (e.g., Wu, 1975).

A comparison of the radial velocity component for each radar station is shown in Fig. 9. The conditions of the collocation are the same as those for the comparison of the current vectors described above. Statistical values of the comparisons are listed in Table 3. For the SY and SR stations, the radial velocity component agrees with the ADCP observations, with rms differences of 26.6 and 25.2 cm s^{-1}, respectively. For the NS station, the data scatter reveals a different trend, with a very low value of the correlation coefficient (0.289). The rms difference increases to 36.6 cm s^{-1}. The magnitude of the radial velocity is underestimated, as indicated by a very low value of the slope (0.289). These are consistent with the result of the buoy comparison in the previous section, indicating that the radial velocity observed at the NS station is less accurate than those at the other stations. Obstacles around the NS station, including a lighthouse and various buildings, might distort the radar antenna pattern and affect the accuracy of measurement. Although we corrected for the distorted antenna pattern using the measured beam pattern of the receiving antenna, the seriously distorted radar antenna pattern might not be fully recov-

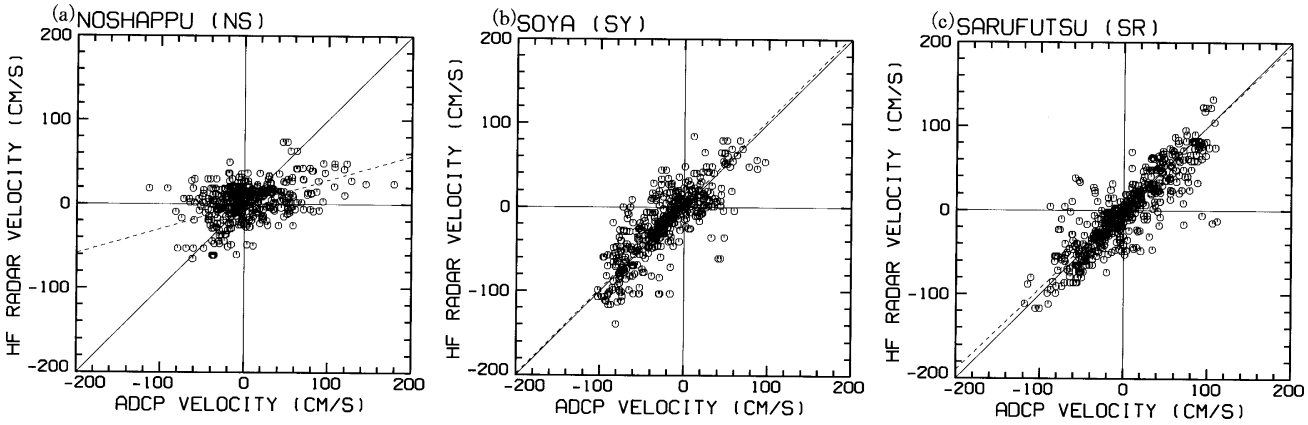

Fig. 9. Comparison of HF radar data with shipboard ADCP observations for radial current velocity. (a) NS, (b) SY, and (c) SR stations. Dashed lines represent the regression lines calculated using the PCA.

Table 4. Statistical values of the comparison of the HF radar current velocity composed with and without data from the NS station with drifting buoy and ADCP observations. Bias is defined as (HF radar – buoy) or (HF radar – ADCP).

	Number of data points	Bias (cm s^{-1})	Rms difference (cm s^{-1})	Correlation coefficient	Slope
Drifting buoys					
With NS station data					
Zonal component	10	–14.23	18.40	0.601	0.849
Meridional component	10	2.49	12.95	0.860	0.914
Without NS station data					
Zonal component	272	4.54	17.14	0.826	0.976
Meridional component	272	1.49	19.75	0.696	0.911
ADCP					
With NS station data					
Zonal component	19	3.62	21.78	0.639	1.028
Meridional component	19	3.30	28.45	0.713	0.897
Without NS station data					
Zonal component	370	–3.64	22.41	0.789	1.012
Meridional component	370	2.87	25.00	0.730	0.853

ered.

Table 4 summarizes the comparison of the HF radar current vectors composed with and without data from the NS station with drifting buoy and ADCP observations. In general, the current vectors derived with and without the radial velocities from the NS station do not show significant deviations, even though very few data points have been derived with data from the NS station. However, Figs. 5 and 9 show that the NS station underestimated the radial current velocity with respect to observations by the drifting buoys and ADCPs. As such, it is concluded that current velocities composed with observations from the NS station, which are mainly located west of 142°E, are less reliable and may be underestimated.

5. Tidal Currents in the Soya Strait

Figure 10 shows stick diagrams (panel (b)) of the surface current vectors at nine representative points in and around the Soya Strait (panel (a)) in August 2003. Diurnal tidal constituents are dominant in this area. Previous studies analyzing current data observed by moored current meters reported that the K1 and O1 constituents are dominant in this area (e.g., Aota and Matsuyama, 1987; Odamaki, 1994). In the region of the SWC (points E, F, H, and I), the surface vectors are mostly aligned to the southeast and the diurnal tidal components have almost the same magnitude as the mean current.

Harmonic analysis with 11 major tidal constituents (Mm, MSf, K1, O1, P1, Q1, M2, S2, N2, K2, 2SM2),

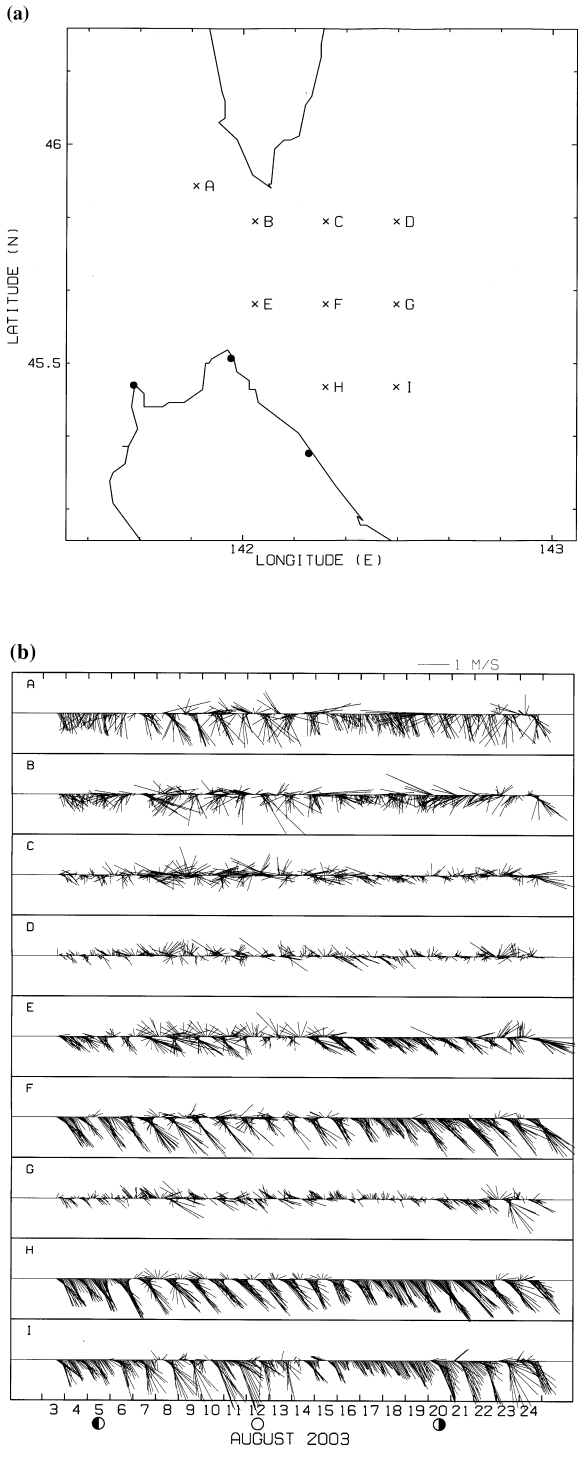

Fig. 10. (a) Locations of nine representative points in and around the Soya Strait, and (b) stick diagrams of the surface current vectors at these points. Symbols at the bottom indicate phases of the fortinightly tidal cycle.

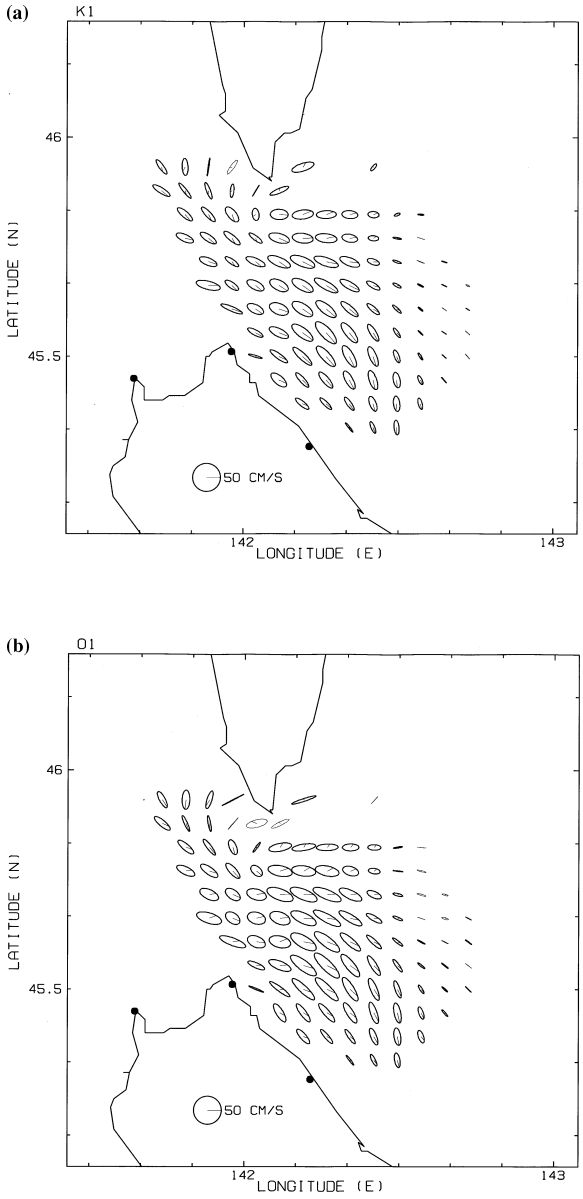

Fig. 11. Tidal current ellipses for the (a) K1 and (b) O1 constituents. The ellipses are drawn for every two grid cells in order to avoid overlap. The thick and thin ellipses denote clockwise and counter-clockwise rotation, respectively. The thin lines in the ellipses represent the phase.

which were selected according to Odamaki (1994), was applied to time series of the surface currents for a 12-month period starting in August 2003. Figure 11 shows the distribution of the calculated tidal current ellipses for the (a) K1 and (b) O1 constituents. In most of the observation area, the tidal current ellipses for both of the constituents are aligned from northwest to southeast and show a clockwise rotation. Spatial variations of the current speed, direction, phase, and ellipticity are very smooth

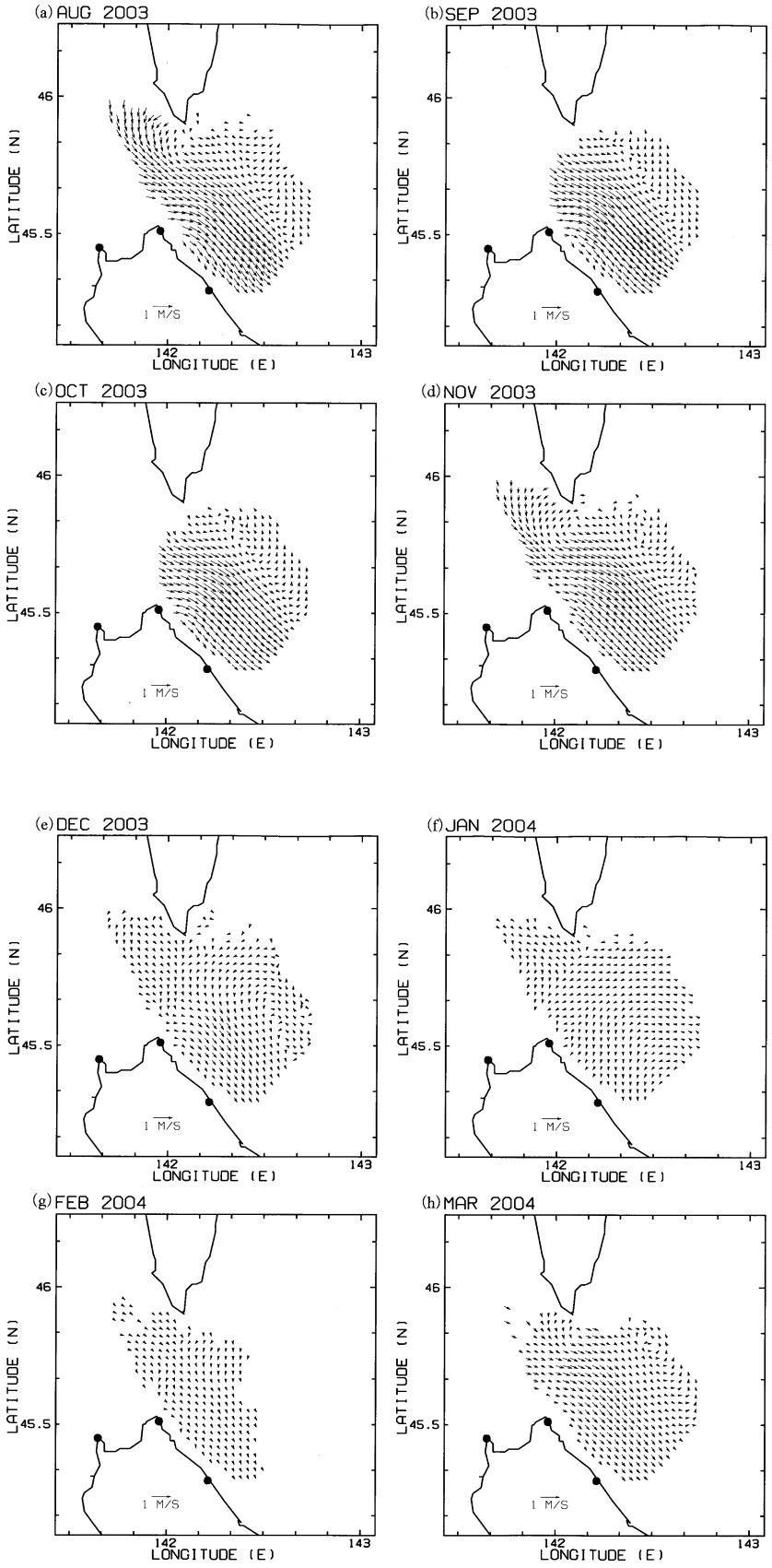

Fig. 12. Monthly-averaged surface current fields from August 2003 to July 2004.

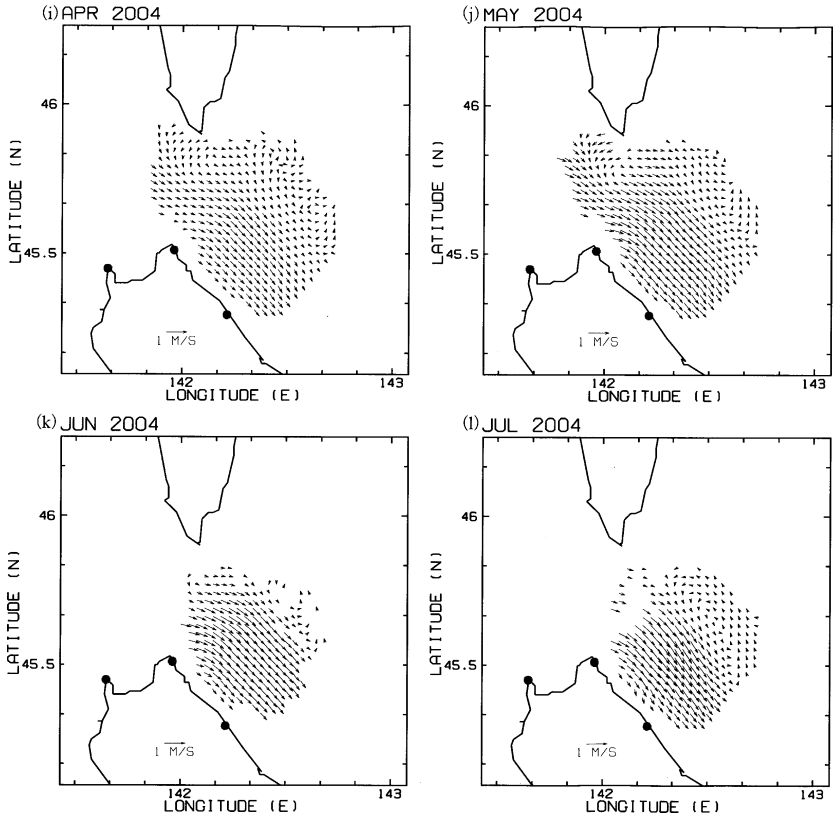

Fig. 12. (continued).

and seem to follow the coastline and bottom topography (Fig. 1(b)). These features are consistent with results of previous studies using data from point-wise observations (e.g., Aota and Matsuyama, 1987; Odamaki, 1994). In an area off Sarufutsu, Odamaki (1994) reported the magnitude of tidal currents as 10 to 20 cm s^{-1} for both of the constituents, which agrees with the result shown in Fig. 11. Odamaki (1994) reported, however, that the long axes of the ellipses for the K1 and O1 constituents reaches 91.5 and 98.2 cm s^{-1}, respectively, in the Soya Strait, and these values are much greater than the results shown in Fig. 11. Underestimation of the radial velocity by the NS station, as discussed in Sections 3 and 4 above, may be a possible reason for the underestimation of the tidal current amplitude in this region, although the results of comparisons in Table 4 do not show such a large underestimation of the amplitude of the current vectors composed with data from the NS station. We also estimated the tidal ellipses from the surface current velocities composed from only the radial velocities measured at the SY and SR stations. The result (not shown here) is almost same as in Fig. 11, and there is still a great difference from the results reported by Odamaki (1994) in the Soya Strait. Further studies are needed to assess the quality of the HF radar data in the strait and to clarify reasons for the discrepancy of tidal amplitudes.

6. Seasonal Variation of the Soya Warm Current

Using the surface current vector fields observed by the HF radars, we now discuss seasonal variations of the SWC. In order to remove the tidal constituents, a 25-hour running average was applied to the time series of the hourly surface current vectors in each grid cell, after which daily and monthly mean current fields were calculated. A 48-hour tide-killer filter (e.g., Thompson, 1983; Hanawa and Mitsudera, 1985), which can more precisely eliminate tidal variations, was not utilized because there were several gaps in the surface current data. The daily and monthly means were not calculated at grid cells in which the number of data obtained was fewer than 15 and 20, respectively. Figure 12 shows the monthly-averaged surface current fields from August 2003 to July 2004. Current data in the Soya Strait are missing for some months because NS station observations were interrupted for a variety of reasons, and the current fields were composed using data from the other two stations only. Data in the eastern part of the current field are missing in February because this area was partly covered by sea ice.

In panels (a)–(d) and (h)–(l) of Fig. 12, the SWC is shown to flow from west to east across the Soya Strait and to turn toward the southeast along the coast, as shown in Fig. 2. The surface current in a region between the SY and SR stations is stronger than that in the Soya Strait. Even though there is a possibility that the influence of underestimation of the radial current velocity at the NS station, as described in Sections 3 and 4 above, may cause a reduction in the current speed in the strait, the effect of bottom topography is a possible reason for the acceleration of the current in this region. The SWC shows a clear seasonal variation, being stronger in summer (August–November) and almost disappearing in winter (December–February). The maximum current speed exceeds 1 m s^{-1} in a region east of the SY station. Since the surface current velocity observed by the HF radars includes the wind drift, the monthly-averaged current fields shown in Fig. 12 also include some contribution from the wind drift components due to the seasonally prevailing winds.

Along the west coast of Sakhalin a southward current is discernible in August (a) and November (d). Although the existence of this southward current has been predicted by numerical experiments (e.g., Ohshima and Wakatsuchi, 1990; Ohshima, 1994), no direct observations have been reported. This southward current also shows clear seasonal variations, and its maximum velocity reaches approximately 60 cm s^{-1} in August. The underestimation of the radial velocity at the NS station is anticipated to have an effect on this region. However, the qualitative features of the southward current may not be affected, since the current direction coincides approximately with the line of sight of the NS station and the magnitude of the current speed is sufficiently robust.

Daily southeastward current components across Line-A (Fig. 1), located off Hama-Onishibetsu, were averaged monthly and are shown with standard deviations in Fig. 13. This line was selected since the surface current velocity of the SWC is strongest in this area (Fig. 12) and is free from the underestimation of the radial velocity at the NS station. The monthly mean profiles also show a clear seasonal variation. The velocity of the SWC reaches its maximum of approximately 1 m s^{-1} in the summer (August and September) and becomes weak in the winter (January and February). The current axis is located 20 to 40 km from the coast in this region, and the typical width of the SWC is approximately 50 km. These features of the SWC are consistent with the results of short-term or point-wise observations reported in previous studies (Aota, 1984; Matsuyama *et al.*, 1999).

Daily surface transport across Line-A was defined

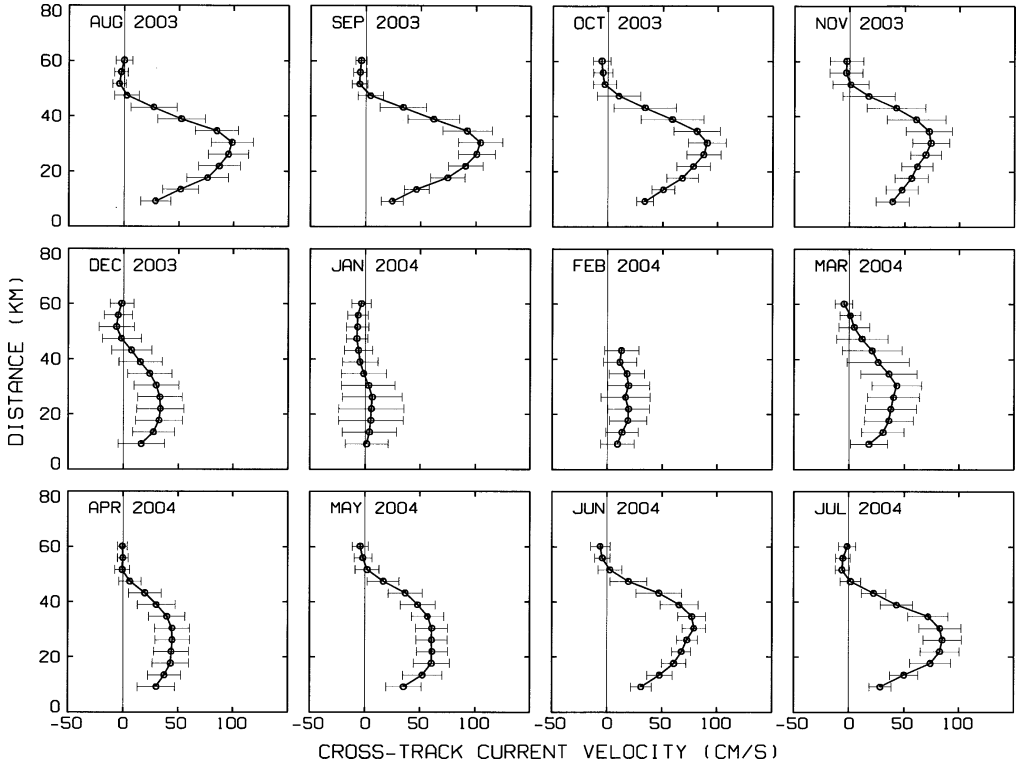

Fig. 13. Monthly-averaged profiles of the southeastward current velocity component across Line-A (Fig. 1) with respect to the distance from the coast line.

by the integration of the daily southeastward current component along the line from the coast to a point at which the component becomes negative. If the current components were positive at all grid cells along the line, the integration was truncated at the farthest point (approximately 60 km from the coast). Figure 14 shows the time series of the surface transport (thick line). Note that the unit of surface transport is not volume/time but area/time, because the HF radars provide only the surface current velocity. Assuming a barotropic flow structure, if the surface transport is multiplied by a depth of 30 to 50 m (Aota, 1984), the maximum volume transport is roughly estimated to range up to 1×10^6 to 2×10^6 m^3s^{-1} (1 to 2 Sv) as daily averages. Data are often absent during the winter (from January to March) because the observation region is covered by sea ice. The surface transport clearly shows a seasonal variation in which the maximum surface transport occurs in summer and the minimum surface transport occurs in winter. As monthly averages, the maximum and minimum surface transports are observed to be 2.6×10^4 m^2s^{-1} in September 2003 and 3.6×10^3 m^2s^{-1} in January 2004, respectively. The mean surface transport during this one-year period is 1.8×10^4 m^2s^{-1}. Assuming a depth of 40 m, these values correspond to volume transports of 1.0, 0.1, and 0.7 Sv, respectively.

The driving force of the SWC is ascribed to the sea level difference between the Sea of Japan and the Sea of Okhotsk (Aota, 1984; Ohshima, 1994). The surface velocity of the SWC has been reported to be closely related to the sea level difference (Aota, 1984; Matsuyama *et al.*, 1999). For comparison with the surface transport as observed by the HF radars, we calculated the sea level difference between two tide gauge stations, Wakkanai (labeled as WK in Fig. 1) and Abashiri (AB in Fig. 1), which represents the sea level difference between the Sea of Japan and the Sea of Okhotsk. A 48-hour tide-killer filter developed by Hanawa and Mitsudera (1985) was applied to the hourly tide gauge records at these stations in order to eliminate the tidal variation precisely. The daily-mean sea levels were then calculated, and atmospheric pressure correction was performed using the daily-mean sea level pressure observed at weather stations in the cities of Wakkanai and Abashiri. The time series is shown by a thin line in Fig. 14. The surface transport of the SWC and the sea level difference show a good correlation with a correlation coefficient of 0.762. Both time series exhibit not only seasonal variation but also variations with time scales of approximately 10 days and a few months. The results shown in Fig. 14 confirm the correlation at various time scales between the SWC and the sea level difference. These results confirm that the SWC is driven by the sea level difference between the Sea of Japan and the Sea of Okhotsk. The response time of the SWC to the change in the sea level difference is considered to be shorter than approximately 10 days, since the both time series show coherent variation up to this temporal scale.

7. Summary and Concluding Remarks

In order to monitor the Soya Warm Current (SWC), three HF ocean radar stations were installed around the Soya/La Perouse Strait. Surface current velocity as observed by the radars was compared with data collected using drifting buoys and shipboard ADCPs. The current

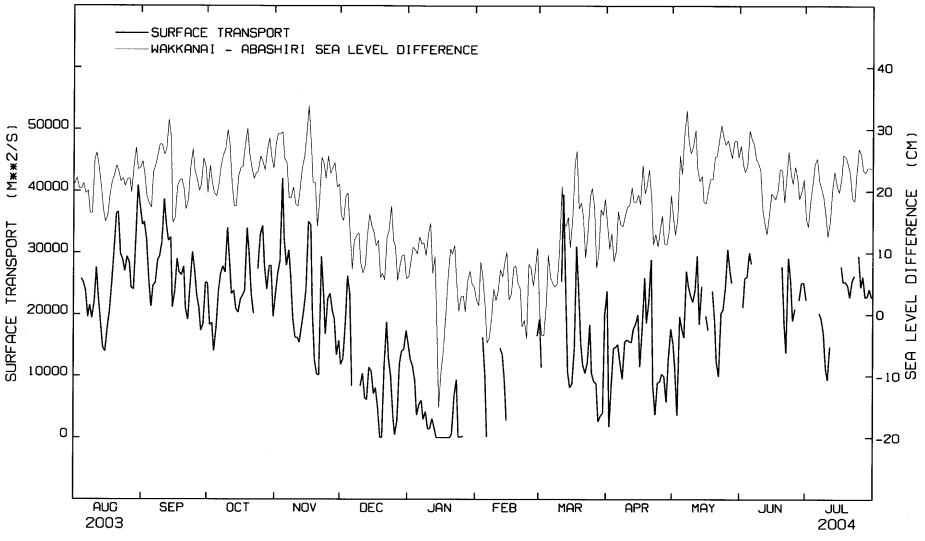

Fig. 14. Daily surface transport of the SWC across Line-A (thick line) and sea-level difference between Wakkanai and Abashiri (thin line).

velocity derived from the radars was shown to agree well with that observed by the drifting buoys. The bias is negligibly small and rms differences are less than 20 cm s^{-1} for both zonal and meridional components in the buoy comparison. The observed velocity also exhibits a reasonable agreement with the shipboard ADCP data, even though the rms differences are slightly increased due to the difference in observation depths of the ADCP and HF radar. The HF radars clearly capture the seasonal variations of the SWC. The velocity of the SWC reaches its maximum, approximately 1 m s^{-1}, in the summer, and becomes weaker in the winter. The surface transport by the SWC shows a significant correlation with the sea level difference along the strait as derived from coastal tide gauge records at Wakkanai and Abashiri, both seasonally, and for time scales of 10 days and a few months.

We have shown here that the HF radar system is an excellent tool for continuous monitoring of the SWC. We intend to extend the time series of the surface current field for several years in order to examine the robustness of the seasonal variation reported here, and to discuss interannual variations of the SWC. As discussed in Sections 3 and 4, improved measurement at the NS station is required in order to obtain more reliable current data, especially in the Soya Strait. Further investigations are also needed to explain the differences in the observed tidal currents between the HF radar and previous studies based on observations using moored current meters as described in Section 5. In Section 6 we discussed the variations of SWC using the surface transport derived from the HF radar observations. However, assessment of the water exchange between the Sea of Japan and the Sea of Okhotsk requires information on the volume transport, which cannot be directly inferred from the surface observations by the HF radars only. A long-term mooring observation program using an upward ADCP is now underway in this region in order to obtain the vertical structures of the SWC and their variations, which will be used to estimate the volume transport from the surface current vectors through empirical relationships.

Acknowledgements

The authors wish to thank the captains and crew of the R/V Hokuyo-maru and the Oyashio-maru, and Iori Tanaka, Shiro Takayanagi, Hideo Yoshida, and Tomohiro Ohtsuki of the Hokkaido Central Fisheries Experimental Station and the Hokkaido Wakkanai Fisheries Experimental Station for their cooperation in deploying the drifting buoys. The authors would also like to thank the Hydrographic and Oceanographic Department of the 1st Regional Coast Guard Headquarters of Japan for providing the ADCP data. The tide gauge records and meteorological data used in the present study were downloaded from the website of the Japan Meteorological Agency. Thanks are also extended to Akira Masuda, Yutaka Yoshikawa, Akira Okuno, Kenji Marubayashi, and Michiyoshi Ishibashi of the Research Institute for Applied Mechanics (RIAM) of Kyushu University, Satoshi Fujii of University of the Ryukyus, Akitugu Nadai of the National Institute of Information and Communications Technology (NICT), and Yasushi Fujiyoshi of the Institute of Low Temperature Science of Hokkaido University for their advice with respect to the design, construction, and operation of the HF radar system. The present study was supported in part by a Grant-in-Aid for Scientific Research (B) (No. 15340152) from the Ministry of Education, Culture, Sports, Science and Technology of Japan.

References

Aota, M. (1984): Oceanographic structure of the Soya Warm Current. *Bull. Coast. Oceanogr.*, **22**, 30–39 (in Japanese).

Aota, M. and M. Matsuyama (1987): Tidal current fluctuations in the Soya Current. *J. Oceanogr. Soc. Japan*, **43**, 276–282.

Barrick, D. E. and B. J. Lipa (1997): Evolution of bearing determination of HF current mapping radars. *Oceanography*, **10**, 72–75.

Barrick, D. E., M. W. Evans and B. L. Weber (1977): Ocean surface currents mapped by radar. *Science*, **198**, 138–144.

Chapman, R. D. and H. C. Graber (1997): Validation of HF radar measurements. *Oceanography*, **10**, 76–79.

Chapman, R. D., L. K. Shay, H. C. Graber, J. B. Edson, A. Karachintsev, C. L. Trump and D. B. Ross (1997): On the accuracy of HF surface current measurements: intercomparisons with ship-based sensors. *J. Geophys. Res.*, **102**, 18,737–18,748.

Graber, H. C., B. K. Haus, L. K. Shay and R. D. Chapman (1997): HF radar comparisons with moored estimates of current speed and direction: expected differences and implications. *J. Geophys. Res.*, **102**, 18,749–18,766.

Hanawa, K. and H. Mitsudera (1985): On the data processing of daily mean values of oceanographic data.—Note on the daily mean sea-level data. *Bull. Coast. Oceanogr.*, **23**, 79–87 (in Japanese).

Holbrook, J. R. and A. S. Frisch (1981): A comparison of near-surface CODAR and VACM measurements in the strait of Juan De Fuca, August 1978. *J. Geophys. Res.*, **86**, 10,908–10,912.

Lawrence, D. J. and P. C. Smith (1986): Evaluation of HF ground-wave radar on the east coast of Canada. *IEEE J. Oceanic Eng.*, **OE-11**, 246–250.

Lipa, B. J. and D. E. Barrick (1983): Least-squares method for the extraction of surface currents from CODAR crossed-loop data: Applications at ARSLOE. *IEEE J. Ocean. Eng.*, **OE-8**, 226–253.

Matsuyama, M., M. Aota, I. Ogasawara and S. Matsuyama (1999): Seasonal variation of Soya Current. *Umi no Kenkyu*, **8**, 333–338 (in Japanese with English abstract and captions).

Nadai, A., H. Kuroiwa, M. Mizutori and S. Sakai (1997): Measurement of ocean surface currents by CRL HF ocean surface radar of the FMCW type. Part 1. Radial current velocity. *J. Oceanogr.*, **53**, 325–342.

Nadai, A., H. Kuroiwa, M. Mizutori and S. Sakai (1999): Measurement of ocean surface currents by CRL HF ocean surface radar of the FMCW type. Part 2. Current vector. *J. Oceanogr.*, **55**, 13–30.

Odamaki, M. (1994): Tides and tidal currents along the Okhotsk coast of Hokkaido. *J. Oceanogr.*, **50**, 265–279.

Ohshima, K. I. (1994): The flow system in the Sea of Japan caused by a sea level difference through shallow straits. *J. Geophys. Res.*, **99**, 9925–9940.

Ohshima, K. I. and M. Wakatsuchi (1990): A numerical study of barotropic instability associated with the Soya Warm Current in the Sea of Okhotsk. *J. Phys. Oceanogr.*, **20**, 570–584.

Prandle, D. (1991): A new view of near-shore dynamics based on observations from HF radar. *Prog. Oceanogr.*, **27**, 403–438.

Stewart, R. H. and J. W. Joy (1974): HF radio measurements of surface currents. *Deep-Sea Res.*, **21**, 1039–1049.

Takeoka, H., Y. Tanaka, Y. Ohno, Y. Hisaki, A. Nadai and H. Kuroiwa (1995): Observation of the Kyucho in the Bungo Channel by HF radar. *J. Oceanogr.*, **51**, 699–711.

Talley, L. D. (1991): An Okhotsk Sea water anomaly: implications for ventilation in the North Pacific. *Deep-Sea Res., Part A*, **38**, Suppl., S171–S190.

Thompson, R. O. R. Y. (1983): Low-pass filters to suppress inertial and tidal frequencies. *J. Phys. Oceanogr.*, **13**, 1077–1083.

Wu, J. (1975): Wind-induced drift current. *J. Fluid Mech.*, **68**, 49–70.

Yasuda, I. (1997): The origin of the North Pacific Intermediate Water. *J. Geophys. Res.*, **102**, 448-465.